Robust Deadbeat Predictive Power Control With a Discrete-Time Disturbance Observer for PWM Rectifiers Under Unbalanced Grid Conditions

Haitao Yang, *Student Member, IEEE*, Yongchang Zhang, *Senior Member, IEEE*, Jiejunyi Liang, Jie Liu, Nong Zhang, and Paul D. Walker

***Abstract*—This paper presents a robust deadbeat predictive power control (DPPC) for pulsewidth modulation (PWM) rectifiers with the consideration of parameter mismatches under unbalanced grid conditions. First, conventional DPPC is modified to extend its application to both ideal and unbalanced grid conditions. Second, a tracking error of the modified DPPC with inaccurate grid-side impedance is analyzed. Third, a discrete-time power disturbance observer (DPDO) is designed to achieve accurate power control with mismatched parameters. The designed DPDO can predict complex power at the next sampling instant and estimate system disturbance simultaneously. Therefore, the DPDO can contribute to eliminate the steady-state tracking error resulting from disturbances caused by inaccurate parameters and compensate one-step delay in digital implementation. Although satisfactory steady-state performance can be obtained with modified DPPC and DPDO, transient performance still deteriorates significantly with an inaccurate value of the grid-side inductance. Thus, an online adaptive method to estimate mismatched inductance is finally developed based on the proposed DPDO. Both DPPC and DPDO are implemented in the stationary reference frame without coordinate transformation. Theoretical analysis confirms that the proposed DPDO can track disturbance without phase lag or magnitude error. Experimental tests and comparative studies with a prior DPPC on a two-level PWM rectifier validate the effectiveness of the proposed scheme.**

***Index Terms*—Parameter estimation, predictive control, pulsewidth modulation (PWM) rectifiers, unbalanced grid.**

Manuscript received July 7, 2017; revised September 12, 2017, October 31, 2017, and January 11, 2018; accepted March 13, 2018. Date of publication March 15, 2018; date of current version November 19, 2018. This work was supported in part by the National Natural Science Foundation of China under Grant 51577003 and in part by the Beijing Natural Science Foundation under Grant 3162012. This paper was presented in part at the IEEE Energy Conversion Congress and Exposition, Cincinnati, OH, USA, 2017. Recommended for publication by Associate Editor G. Escobar. *(Corresponding author: Yongchang Zhang.)*

H. Yang, J. Liang, N. Zhang and P. D. Walker are with the Faculty of Engineering and Information Technology, University of Technology Sydney, Ultimo, NSW 2007, Australia (e-mail:

To address deteriorated control performance caused by parameter mismatches for predictive control, different online correction methods can be found in the literature. In [19], the effects of model uncertainty are studied, and then, a least-squares estimation is designed to update model parameters. In [20], the grid-side inductance is estimated by comparing magnitudes of the calculated grid voltages within two sampling periods. However, since the magnitude of the grid voltage vector is not a constant for unbalanced three-phase voltages, this method cannot be directly applied to unbalanced networks. Other techniques, such as evaluating tracking error of reactive power [21] and injecting test signals [22], can also be employed to get actual model parameters. Apart from parameter adaption, disturbance observers are also employed in many studies to improve control accuracy. A Luenberger observer is designed in [13] and [23] to improve robustness of predictive control. Both schemes are implemented in a synchronous reference frame. A PI observer is proposed in [24] for a one-step-ahead predictor without offset during steady-state operation. Since an integrator cannot track ac disturbances without phase lag and magnitude error, this scheme should be implemented in the synchronous reference frame as that in [13] for three-phase VSRs. However, for those control schemes implemented in the stationary reference frame (e.g., DPPCs in [10] and [18]), it is preferable to design a disturbance observer in the stationary reference frame.

For DBC of power converters, both current vector and complex power can be selected as control variables. In most of the previous research [13], [24]–[26], disturbance observers are designed based on the measured current. Few have considered a disturbance observer constructed based on the complex power. Moreover, they are usually designed assuming an ideal grid. Hence, their feasibility in unbalanced grid conditions needs to be further verified. As these disturbance observers are usually implemented in the synchronous reference frame, they cannot be simply integrated into control schemes implemented in the stationary reference frame. There are some observers designed for unbalanced network, such as those presented in [27]–[29]. However, they are usually used for estimating or predicting fundamental and harmonic components of grid voltages. Using an observer to estimate disturbances caused by mismatched parameters under unbalanced grid conditions in the stationary reference frame still needs to be investigated.

In practical application, it is necessary to ensure that the PWM rectifier could work properly under both ideal and unbalanced grid conditions. For a weak grid, unbalanced grid condition with 15% single-phase voltage sag is very common [30]. Considering that severely unbalanced conditions may occur due to grid fault, highly imbalanced load, etc., more severe voltage sags such as 50% and 90% voltage dips in a single phase are experimentally investigated in [31]. In this paper, the disturbance observer and DPPC presented in [32], which can only work properly under ideal grid conditions, are revised to extend their application under unbalanced grid conditions. In [32], the DPDO is designed and analyzed in the continuous-time domain with subsequent discretization for practical implementation. In this paper, the DPDO is developed in the discrete-time domain for the three-phase three-wire converter system. As the discrete nature of the digital controller is directly considered in the design phase, more accurate analytical results and simplified implementation process are achieved. Furthermore, the guidelines for choosing observer parameters are developed, and an online adaptive method for inductance estimation is proposed to further improve the dynamic performance. For the proposed DPDO-based DPPC, the estimation of disturbances caused by mismatched parameters is integrated into a one-step-ahead prediction procedure. As such, one-step delay compensation and disturbance estimation can be achieved simultaneously. Therefore, the proposed scheme would not substantially increase complexity compared to a standard DPPC. Experimental results and comparative research with a prior method [18] justify the effectiveness of the proposed method.

II. Dynamic Equations of a VSR

For a three-phase three-wire PWM rectifier, its mathematical model in the stationary $\alpha\beta$ reference frame can be expressed in the complex vector form as

$$L_g \frac{d\boldsymbol{i}_g}{dt} = \boldsymbol{u}_g - \boldsymbol{u}_c - R_g \boldsymbol{i}_g \tag{1}$$

where $\boldsymbol{u}_g = u_{g\alpha} + ju_{g\beta}$, $\boldsymbol{u}_c = u_{c\alpha} + ju_{c\beta}$, and $\boldsymbol{i}_g = i_{g\alpha} + ji_{g\beta}$ are the grid voltage vector, the converter voltage vector, and the grid current vector, respectively; and L_g and R_g are the inductance and the resistance of the grid-side filter, respectively. The grid-side complex power $\boldsymbol{S}$ can be calculated as

$$\boldsymbol{S} = P + jQ = 1.5\boldsymbol{i}_g^* \boldsymbol{u}_g \tag{2}$$

where P and Q are active and reactive powers, respectively, and the superscript $*$ denotes the conjugate of a complex vector.

For unbalanced grid voltages, $\boldsymbol{u}_g$ can be decomposed into the fundamental positive-sequence component (FPSC) $\boldsymbol{u}_{gp}$ and the fundamental negative-sequence component (FNSC) $\boldsymbol{u}_{gn}$ as

$$\boldsymbol{u}_g = \boldsymbol{u}_{gp} + \boldsymbol{u}_{gn}. \tag{3}$$

The zero-sequence component is omitted in (3) because it has no effect on power control for a three-phase three-wire converter system [31]. Similarly, the grid current $\boldsymbol{i}_g$ can be written as

$$\boldsymbol{i}_g = \boldsymbol{i}_{gp} + \boldsymbol{i}_{gn}. \tag{4}$$

With the grid voltage in (3) and the current controlled as shown in (4), the instantaneous power can be calculated as

$$\begin{bmatrix} P \\ Q \end{bmatrix} = \begin{bmatrix} \overline{P} + P_c \cos(2\omega_g t) + P_s \sin(2\omega_g t) \\ \overline{Q} + Q_c \cos(2\omega_g t) + Q_s \sin(2\omega_g t) \end{bmatrix} \tag{5}$$

where $\overline{P}$ and $\overline{Q}$ are average values of the active and reactive powers, respectively, and P_c, P_s and Q_c, Q_s are ripple components of P and Q, respectively. As derived in [2], the average value and ripple components of P and Q can be further expressed as

$$\overline{P} = \frac{3}{2}\left(\boldsymbol{i}_{dq}^{+} \odot \boldsymbol{e}_{dq}^{+} + \boldsymbol{i}_{dq}^{-} \odot \boldsymbol{e}_{dq}^{-}\right) \tag{6}$$

$$P_c = \frac{3}{2}\left(\boldsymbol{i}_{dq}^{+} \odot \boldsymbol{e}_{dq}^{-} + \boldsymbol{i}_{dq}^{-} \odot \boldsymbol{e}_{dq}^{+}\right) \tag{7}$$

$$P_s = \frac{3}{2}\left(\boldsymbol{i}_{dq}^{+} \otimes \boldsymbol{e}_{dq}^{-} - \boldsymbol{i}_{dq}^{-} \otimes \boldsymbol{e}_{dq}^{+}\right) \tag{8}$$

$$\overline{Q} = \frac{3}{2}\left(\boldsymbol{i}_{dq}^{+} \otimes \boldsymbol{e}_{dq}^{+} + \boldsymbol{i}_{dq}^{-} \otimes \boldsymbol{e}_{dq}^{-}\right) \tag{9}$$

$$Q_c = \frac{3}{2}\left(\boldsymbol{i}_{dq}^{+} \otimes \boldsymbol{e}_{dq}^{-} + \boldsymbol{i}_{dq}^{-} \otimes \boldsymbol{e}_{dq}^{+}\right) \tag{10}$$

$$Q_s = \frac{3}{2}\left(\boldsymbol{i}_{dq}^{-} \odot \boldsymbol{e}_{dq}^{+} - \boldsymbol{i}_{dq}^{+} \odot \boldsymbol{e}_{dq}^{-}\right) \tag{11}$$

where $\odot$ and $\otimes$ denote the dot product and the cross product of two complex vectors, respectively, $\boldsymbol{i}_{dq}^{+}$ and $\boldsymbol{e}_{dq}^{+}$ represent FPSCs of the grid current and the grid voltage in the positive-sequence synchronous reference frame, and $\boldsymbol{i}_{dq}^{-}$ and $\boldsymbol{e}_{dq}^{-}$ denote FNSCs in the negative-sequence synchronous reference frame. It is clear that there are four controllable freedoms (i_d^{+}, i_d^{-}, i_q^{+}, and i_q^{-}). This implies only four control targets can be established [31]. In most of the applications, the average active and reactive powers are controlled to follow their references, i.e.,

$$\overline{P} = P^{\mathrm{ref}} \tag{12}$$

$$\overline{Q} = Q^{\mathrm{ref}}. \tag{13}$$

The remaining two control functions can be selected as one of the following:

1) eliminating active power ripples, i.e., $P_c = 0$ and $P_s = 0$. In this case, Q_c and Q_s leave to be uncontrolled and thus reactive power ripples exist under unbalanced grid conditions [2];
2) eliminating reactive power ripples, i.e., $Q_c = 0$ and $Q_s = 0$. In this case, P_c and P_s are uncontrolled and thus there are active power ripples;
3) achieving balanced and sinusoidal input currents, i.e., $i_d^{-} = 0$ and $i_q^{-} = 0$. In this case, only two control freedoms (i_d^{+} and i_q^{+}) are available, which can only be used for satisfying (12) and (13). As P_c, P_s and Q_c, Q_s are all uncontrolled, both active and reactive powers exhibit power oscillations if grid voltages are unbalanced [31].

As stated above, all control objectives have their own merits and drawbacks under unbalanced grid conditions. To ensure a fair comparison with [2] and verify the effectiveness of the proposed DPDO, the same control objective of eliminating active power ripples as in [2] is selected in this paper.

The quadrature component of the grid voltage vector lagging actual grid voltage vector by 90° can be expressed as [2]

$$\boldsymbol{u}_g^{'} = -j\boldsymbol{u}_{gp} + j\boldsymbol{u}_{gn}. \tag{14}$$

Based on (3) and (14), the derivative of the grid voltage vector can be expressed by

$$\begin{aligned}\frac{d\boldsymbol{u}_g}{dt} &= \frac{d\boldsymbol{u}_{gp}}{dt} + \frac{d\boldsymbol{u}_{gn}}{dt} = j\omega_g\boldsymbol{u}_{gp} - j\omega_g\boldsymbol{u}_{gn} \\ &= -\omega_g\left(-j\boldsymbol{u}_{gp} + j\boldsymbol{u}_{gn}\right) = -\omega_g\boldsymbol{u}_g^{'}.\end{aligned} \tag{15}$$

With the derivatives of $\boldsymbol{i}_g$ and $\boldsymbol{u}_g$ shown in (1) and (15), the derivative of $\boldsymbol{S}$ can be calculated from (2) as

$$\begin{aligned}\frac{d\boldsymbol{S}}{dt} &= \frac{3}{2}\left(\boldsymbol{u}_g\frac{d\boldsymbol{i}_g^{*}}{dt} + \boldsymbol{i}_g^{*}\frac{d\boldsymbol{u}_g}{dt}\right) \\ &= \frac{1}{L_g}\left[\frac{3}{2}\left(|\boldsymbol{u}_g|^2 - \boldsymbol{u}_c^{*}\boldsymbol{u}_g\right) - \left(R_g + \frac{\omega_g L_g\boldsymbol{u}_g^{'}}{\boldsymbol{u}_g}\right)\boldsymbol{S}\right].\end{aligned} \tag{16}$$

It should be noted that (16) is valid for both ideal and unbalanced grid conditions. For an ideal grid, $\boldsymbol{u}_g^{'} = -j\boldsymbol{u}_g$ holds. In this case, the derivative of complex power is the same as that presented in [18], which is a special case of (16).

With a small sampling period, the simple forward Euler method can be employed to discretize (16). The result is shown as follows:

$$\begin{aligned}\boldsymbol{S}^{k+1} = \boldsymbol{S}^{k} &+ \frac{T_{sc}}{L_g} \\ &\times\left[\frac{3}{2}\left(\left|\boldsymbol{u}_g^{k}\right|^2 - \left(\boldsymbol{u}_c^{k}\right)^{*}\boldsymbol{u}_g^{k}\right) - (R_g + \omega_g L_g J^{k})\boldsymbol{S}^{k}\right]\end{aligned} \tag{17}$$

where the superscript k represents the variable at the kth instant, T_{sc} is the sampling period, and $J^{k} = \left(\boldsymbol{u}_g^{'}\right)^{k}/\boldsymbol{u}_g^{k}$.

III. Deadbeat Predictive Power Control

A. Reference Compensation for Unbalanced Grid Voltages

In this paper, the control objectives under unbalanced grid conditions are selected as keeping instantaneous active power constant and grid currents sinusoidal. As stated in [2], this can be achieved by adding an imaginary part to the original reference of complex power. The compensation of power reference can be expressed as follows:

$$\boldsymbol{S}^{\mathrm{com}} = j\frac{\boldsymbol{u}_g \odot \boldsymbol{u}_g^{'}}{\boldsymbol{u}_g \otimes \boldsymbol{u}_g^{'}}P^{\mathrm{ref}}. \tag{18}$$

A detailed derivation of (18) can be found in [2], and thus, it is not repeated here. As $\boldsymbol{u}_g \odot \boldsymbol{u}_g^{'} = 0$ for an ideal grid, $\boldsymbol{S}^{\mathrm{com}}$ presented in (18) is suitable for both ideal and unbalanced grid conditions. After calculating $\boldsymbol{S}^{\mathrm{com}}$, the reference of complex power can be obtained as

$$\boldsymbol{S}^{\mathrm{ref}} = P^{\mathrm{ref}} + jQ^{\mathrm{ref}} + \boldsymbol{S}^{\mathrm{com}}. \tag{19}$$

The reactive power reference Q^{ref} is set as zero in this paper. However, it can be found from (18) and (19) that an oscillating imaginary component would be added to the original power reference if grid voltages are unbalanced. Hence, after compensation, the reactive power reference oscillates under unbalanced conditions. Substituting (18) into (19), $\boldsymbol{S}^{\mathrm{ref}}$ can be further rewritten as

$$\boldsymbol{S}^{\mathrm{ref}} = P^{\mathrm{ref}}\left(1 + j\frac{\boldsymbol{u}_g \odot \boldsymbol{u}_g^{'}}{\boldsymbol{u}_g \otimes \boldsymbol{u}_g^{'}}\right) \tag{20}$$

$$= jP^{\mathrm{ref}}\frac{\left(\boldsymbol{u}_g^{'}\right)^{*}\boldsymbol{u}_g}{\boldsymbol{u}_g \otimes \boldsymbol{u}_g^{'}}. \tag{21}$$

B. Influence of Mismatched Parameters on Tracking Accuracy

Assuming $\boldsymbol{S}^{k+1}=\boldsymbol{S}^{\mathrm{ref}}$, the converter voltage that forces the complex power to reach its reference at the next sampling period can be obtained from (17) as

$$\boldsymbol{u}_c^k=\boldsymbol{u}_g^k-\frac{2}{3}\left(\frac{(R_g+\omega_g L_g J^k)\boldsymbol{S}^k}{\boldsymbol{u}_g^k}\right)^*-\frac{2L_g}{3T_{sc}}\left(\frac{\boldsymbol{S}^{\mathrm{ref}}-\boldsymbol{S}^k}{\boldsymbol{u}_g^k}\right)^*. \tag{22}$$

One can see that the expression of $\boldsymbol{u}_c^k$ includes parameters of grid-side inductance and resistance, which may vary with time due to saturation, temperature, etc. With mismatched parameters, the actual power would deviate from its reference, reducing the accuracy of power control.

To evaluate the impact of parameter mismatch, the estimated inductance and resistance used in the controller are defined as

$$\hat{L}_g=L_g-\Delta L \tag{23}$$

$$\hat{R}_g=R_g-\Delta R \tag{24}$$

where ΔL and ΔR are the errors of estimated inductance and resistance, respectively. In practical application, $\boldsymbol{u}_c^k$ is calculated with $\hat{L}_g$ and $\hat{R}_g$ as

$$\hat{\boldsymbol{u}}_c^k=\boldsymbol{u}_g^k-\frac{2}{3}\left(\frac{(\hat{R}_g+\omega_g\hat{L}_g J^k)\boldsymbol{S}^k}{\boldsymbol{u}_g^k}\right)^*-\frac{2\hat{L}_g}{3T_{sc}}\left(\frac{\boldsymbol{S}^{\mathrm{ref}}-\boldsymbol{S}^k}{\boldsymbol{u}_g^k}\right)^*. \tag{25}$$

Replacing $\boldsymbol{u}_c^k$ in (17) with the above calculated $\hat{\boldsymbol{u}}_c^k$ yields

$$\boldsymbol{S}^{k+1}=\boldsymbol{S}^k+\frac{T_{sc}}{L_g}\left[-\left((R_g-\hat{R}_g)+\omega_g J^k(L_g-\hat{L}_g)\right)\boldsymbol{S}^k\right]+\frac{\hat{L}_g}{L_g}\left(\boldsymbol{S}^{\mathrm{ref}}-\boldsymbol{S}^k\right). \tag{26}$$

With (23) and (24), (26) can be further simplified as

$$\boldsymbol{S}^{k+1}=\frac{(L_g-\Delta L)\boldsymbol{S}^{\mathrm{ref}}+\left(\Delta L-T_{sc}(\omega_g\Delta L J^k+\Delta R)\right)\boldsymbol{S}^k}{L_g}. \tag{27}$$

It is clear that if ΔL and ΔR are zero, $\boldsymbol{S}^{k+1}$ equals $\boldsymbol{S}^{\mathrm{ref}}$. However, if there is any mismatch, the applied voltage (25) can no longer force $\boldsymbol{S}^{k+1}$ to reach $\boldsymbol{S}^{\mathrm{ref}}$. As conventional DPPC is sensitive to parameter variations, a robust DPPC based on disturbance estimation will be proposed in the following text. Since $\boldsymbol{S}^{k+1}\approx\boldsymbol{S}^k$ during steady-state operation, (27) can be further simplified as

$$\boldsymbol{S}^k=\frac{\boldsymbol{S}^{\mathrm{ref}}}{1+\frac{(\Delta RT_{sc}+\omega_g T_{sc}\Delta L J^k)}{\hat{L}_g}}. \tag{28}$$

In practical application, the grid-side resistance is usually small to reduce power losses. Additionally, the influence of ΔR is multiplied by a small value $\frac{T_{sc}}{\hat{L}_g}$. Hence, the influence of ΔR on power control is usually negligible.

IV. Disturbance Estimation in the Discrete-Time Domain

A. Design of DPDO

According to (17), one-step-ahead prediction can be rearranged using the following equation with the estimated inductance and resistance:

$$\boldsymbol{S}^{k+1}=\boldsymbol{S}^k+\frac{T_{sc}}{\hat{L}_g}\left[\frac{3}{2}\left(\left|\boldsymbol{u}_g^k\right|^2-\left(\boldsymbol{u}_c^k+\boldsymbol{u}_d^k\right)^*\boldsymbol{u}_g^k\right)-(\hat{R}_g+\omega_g\hat{L}_g J^k)\cdot\boldsymbol{S}^k\right] \tag{29}$$

where $\boldsymbol{u}_d$ is the disturbance voltage that compensates the impact of inaccurate parameters so that the responses of (29) are exactly the same as (17). Subtracting (29) from (17) yields

$$\Delta L\cdot\boldsymbol{S}^{k+1}=\Delta L\cdot\boldsymbol{S}^k+\frac{3T_{sc}}{2}\times\left[\left(\boldsymbol{u}_d^k\right)^*\boldsymbol{u}_g^k-(\Delta R+J^k\omega_g\Delta L)\boldsymbol{S}^k\right]. \tag{30}$$

From (30), $\boldsymbol{u}_d^k$ can be solved as

$$\boldsymbol{u}_d^k=\frac{2}{3}\left(\frac{\Delta L\left(\boldsymbol{S}^{k+1}-\boldsymbol{S}^k\right)}{\boldsymbol{u}_g^k T_{sc}}+\frac{(\Delta R+J^k\omega_g\Delta L)\boldsymbol{S}^k}{\boldsymbol{u}_g^k}\right)^*. \tag{31}$$

Similar to $\boldsymbol{u}_g$, $\boldsymbol{u}_d$ can be decomposed into FPSC $\boldsymbol{u}_{dp}$ and FNSC $\boldsymbol{u}_{dn}$ under the unbalanced grid condition. The proof is provided in the Appendix. In the steady state, the dynamics of $\boldsymbol{u}_{dp}$ and $\boldsymbol{u}_{dn}$ can be expressed in the discrete-time domain as

$$\begin{cases}\boldsymbol{u}_{dp}^{k+1} & =e^{j\omega_g T_{sc}}\boldsymbol{u}_{dp}^k\\ \boldsymbol{u}_{dn}^{k+1} & =e^{-j\omega_g T_{sc}}\boldsymbol{u}_{dn}^k.\end{cases} \tag{32}$$

As ΔL and ΔR are unknown, $\boldsymbol{u}_d$ is not directly available. A discrete-time disturbance observer is thus designed based on the system model (29) and (32) as follows:

$$\begin{cases}\hat{\boldsymbol{S}}^{k+1}=\hat{\boldsymbol{S}}^k+\frac{T_{sc}}{\hat{L}_g}\left[\frac{3}{2}\left(\left|\boldsymbol{u}_g^k\right|^2-\left(\boldsymbol{u}_c^k+\hat{\boldsymbol{u}}_d^k+\boldsymbol{u}_o^k\right)^*\boldsymbol{u}_g^k\right)-(\hat{R}_g+\omega_g\hat{L}_g J^k)\cdot\boldsymbol{S}^k\right] & (33.1)\\ \hat{\boldsymbol{u}}_{dp}^{k+1}=e^{j\omega_g T_{sc}}\hat{\boldsymbol{u}}_{dp}^k+\lambda\boldsymbol{u}_o^k & (33.2)\\ \hat{\boldsymbol{u}}_{dn}^{k+1}=e^{-j\omega_g T_{sc}}\hat{\boldsymbol{u}}_{dn}^k+\lambda\boldsymbol{u}_o^k & (33.3)\\ \hat{\boldsymbol{u}}_d^{k+1}=\hat{\boldsymbol{u}}_{dp}^{k+1}+\hat{\boldsymbol{u}}_{dn}^{k+1} & (33.4)\end{cases}$$

where $\boldsymbol{u}_o$ is a control function, $\hat{\boldsymbol{u}}_d$ is the estimation of disturbance voltage $\boldsymbol{u}_d$, $\hat{\boldsymbol{u}}_{dp}$ and $\hat{\boldsymbol{u}}_{dn}$ are FPSC and FNSC decomposed from $\hat{\boldsymbol{u}}_d$, respectively, and λ is a gain for disturbance voltage estimation. Subtracting (29) from (33.1), the following error equation can be obtained:

$$\boldsymbol{e}_s^{k+1}=\boldsymbol{e}_s^k+\frac{T_{sc}}{\hat{L}_g}\left(-\frac{3}{2}\left(\boldsymbol{e}_u^k+\boldsymbol{u}_o^k\right)^*\boldsymbol{u}_g^k\right) \tag{34}$$

where $\boldsymbol{e}_s=\hat{\boldsymbol{S}}-\boldsymbol{S}$ is the error of complex power and $\boldsymbol{e}_u=\hat{\boldsymbol{u}}_d-\boldsymbol{u}_d$ is the error of disturbance voltage. It should be noted that the actual complex power $\boldsymbol{S}^k$ rather than the estimated value $\hat{\boldsymbol{S}}^k$ is used in the last term of (33.1). Such an arrangement can cancel $(\hat{R}_g+\omega_g\hat{L}_g J^k)$ related terms in the error equation (34).

This can significantly facilitate the design process of the observer because J^k is a varying parameter. Setting the estimation error decays exponentially, i.e.,

$$\boldsymbol{e}_s^{k+1} = (1 - qT_{sc})\boldsymbol{e}_s^k \tag{35}$$

where $q > 0$ is a parameter needs to be designed, the following equation can be derived based on (34) and (35):

$$\frac{3}{2}\left(\boldsymbol{e}_u^k + \boldsymbol{u}_o^k\right)^* \boldsymbol{u}_g^k - \hat{L}_g q \boldsymbol{e}_s^k = 0. \tag{36}$$

Considering the estimation error $\boldsymbol{e}_u^k$ as the disturbance, the control function $\boldsymbol{u}_o^k$ is chosen as

$$\boldsymbol{u}_o^k = \frac{2\hat{L}_g q}{3}\left(\frac{\boldsymbol{e}_s^k}{\boldsymbol{u}_g^k}\right)^*. \tag{37}$$

From (34) and (37), the error dynamics can be obtained as

$$\hat{L}_g \boldsymbol{e}_s^{k+1} = \hat{L}_g \boldsymbol{e}_s^k + T_{sc}\left(-\frac{3}{2}\left(\boldsymbol{e}_u^k\right)^* \boldsymbol{u}_g^k - \hat{L}_g q \boldsymbol{e}_s^k\right). \tag{38}$$

According to (38), the following transfer function can be derived:

$$F(z) = \frac{\boldsymbol{e}_s(z)}{\boldsymbol{e}_d(z)} = \frac{3T_{sc}}{2\hat{L}_g}\frac{1}{z - (1 - qT_{sc})} \tag{39}$$

where z is a shift operator and $\boldsymbol{e}_d = -(\boldsymbol{e}_u)^* \boldsymbol{u}_g$. The pole of $F(z)$ is

$$p = 1 - qT_{sc}. \tag{40}$$

To ensure stability, $|p| < 1$ must be satisfied, i.e.,

$$0 < q < \frac{2}{T_{sc}}. \tag{41}$$

Namely, if q satisfies condition (41), the estimator of complex power, as shown in (33), is stable. In the next subsection, the convergence of the observer will be analyzed, and a guideline for selection of q and λ is developed.

B. Analysis of DPDO

First, the relationship between $\hat{\boldsymbol{u}}_d$ and $\boldsymbol{u}_d$ will be analyzed. According to (37) and (39), the following equation can be derived:

$$H(z) = \frac{\boldsymbol{u}_o(z)}{(\boldsymbol{u}_d(z) - \hat{\boldsymbol{u}}_d(z))} = \frac{qT_{sc}}{z - (1 - qT_{sc})}. \tag{42}$$

It can be seen that $\boldsymbol{u}_o$ is a low-pass-filtered value of $\boldsymbol{e}_u$. As estimated disturbance voltages $\hat{\boldsymbol{u}}_{dp}$ and $\hat{\boldsymbol{u}}_{dn}$ are reconstructed based on $\boldsymbol{u}_o$, larger q is required for faster dynamic performance. On the other hand, smaller q is preferable for better noise immunity.

From (33.2) and (33.3), $\boldsymbol{u}_o$ can be expressed as

$$\boldsymbol{u}_o(z) = \frac{z - e^{j\omega_g T_{sc}}}{\lambda}\hat{\boldsymbol{u}}_{dp}(z) \tag{43}$$

$$\boldsymbol{u}_o(z) = \frac{z - e^{-j\omega_g T_{sc}}}{\lambda}\hat{\boldsymbol{u}}_{dn}(z). \tag{44}$$

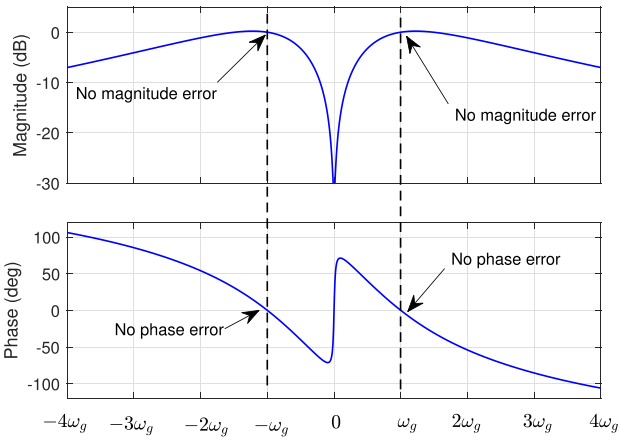

Fig. 1. Bode diagram of $J(z)$.

Based on (42)–(44), and considering that $\hat{\boldsymbol{u}}_d = \hat{\boldsymbol{u}}_{dp} + \hat{\boldsymbol{u}}_{dn}$, the relationship between $\hat{\boldsymbol{u}}_d$ and its actual value $\boldsymbol{u}_d$ is given as

$$J(z) = \frac{\hat{\boldsymbol{u}}_d(z)}{\boldsymbol{u}_d(z)} = \frac{2G(z - \cos(\omega_g T_{sc}))}{z^2 + 2\left(G - \cos(\omega_g T_{sc})\right)z + 1 - 2G\cos(\omega_g T_{sc})} \tag{45}$$

where

$$G = \frac{\lambda q T_{sc}}{z - (1 - qT_{sc})}. \tag{46}$$

With a small sampling period, $\cos(\omega_g T_{sc}) \approx 1$. Then, the pole of $J(z)$ can be calculated as

$$p^{1,2} = 1 - \frac{qT_{sc} \pm \sqrt{-qT_{sc}(8\lambda - qT_{sc})}}{2}. \tag{47}$$

If

$$8\lambda - qT_{sc} = qT_{sc} \tag{48}$$

$p^{1,2}$ can be simplified as

$$p^{1,2} = \left(1 - \frac{qT_{sc}}{2}\right) \pm j\frac{qT_{sc}}{2}. \tag{49}$$

According to (49) and considering $e^{-\frac{qT_{sc}}{2}} \approx 1 - \frac{qT_{sc}}{2}$, the damping ratio can be set as $\sqrt{2}/2 \approx 0.707$ by satisfying (48). The settling time can be subsequently calculated as [33]

$$t_s = \frac{4T_{sc}}{-\ln(1 - qT_{sc}/2)} \approx \frac{8}{q}. \tag{50}$$

Once q is obtained according to the desired settling time t_s, λ can be solved from (48) as

$$\lambda = \frac{qT_{sc}}{4}. \tag{51}$$

Fig. 1 shows the bode diagram of $J(z)$. One can see that there is no magnitude and phase error at fundamental positive frequency and fundamental negative frequency. Namely, $\hat{\boldsymbol{u}}_d$ could track

FPSC and FNSC of $\boldsymbol{u}_d$ accurately. Meanwhile, the dc offset and high-frequency noises can be suppressed.

Then, the estimation error of complex power is analyzed. For a constant $\boldsymbol{e}_d$, the final value of $\boldsymbol{e}_s$ can be solved from (39) as

$$\lim_{k\to\infty}\boldsymbol{e}_s^k=\lim_{z\to 1}(1-z^{-1})\left(\frac{3T_{sc}}{2\hat{L}_g}\frac{1}{z-(1-qT_{sc})}\frac{\boldsymbol{e}_d}{1-z^{-1}}\right)=\frac{3\boldsymbol{e}_d}{2\hat{L}_g q}. \tag{52}$$

It has been shown that $\hat{\boldsymbol{u}}_d$ could track $\boldsymbol{u}_d$ without an error. Once $\hat{\boldsymbol{u}}_d$ equals $\boldsymbol{u}_d$, $\boldsymbol{e}_d=0$. According to (52), the estimation error of complex power $\boldsymbol{e}_s$ would be finally zero, i.e., the estimated complex power can converge to its actual value.

C. Inductance Estimation Based on DPDO

As can be seen from (31), a derivative term of complex power related to ΔL exists in $\boldsymbol{u}_d$. Consequently, a large disturbance would occur during the transient process, e.g., during step responses. This would lead to deteriorated dynamic performance of DPPC. Hence, it is necessary to estimate ΔL online for better dynamic performance.

According to (21) and (76) derived in the Appendix, $\boldsymbol{u}_d^k$ can be calculated as

$$\boldsymbol{u}_d^k=\frac{2\omega_g\Delta L}{3}\left(\frac{\boldsymbol{S}^k\left(\frac{\boldsymbol{u}_g^k}{\left(\boldsymbol{u}_g'\right)^k}\right)^*}{\boldsymbol{u}_g^k}\right)^*+\frac{2}{3}\Delta R\left(\frac{\boldsymbol{S}^k}{\boldsymbol{u}_g^k}\right)^*. \tag{53}$$

According to (53), multiplying the conjugate of the $\boldsymbol{u}_d^k$ with $\boldsymbol{u}_g^k$ yields the following equation:

$$\left(\boldsymbol{u}_d^k\right)^*\boldsymbol{u}_g^k=\frac{2\omega_g\Delta L}{3}\boldsymbol{S}^k\left(\frac{\boldsymbol{u}_g^k}{\left(\boldsymbol{u}_g'\right)^k}\right)^*+\frac{2}{3}\Delta R\boldsymbol{S}^k. \tag{54}$$

To calculate the mismatched inductance from (54), ΔR-related terms must be eliminated to avoid its influence on the inductance estimation. Considering $\boldsymbol{S}^k\otimes\boldsymbol{S}^k=0$, the following equation can be easily obtained from (54):

$$\left(\left(\boldsymbol{u}_d^k\right)^*\boldsymbol{u}_g^k\right)\otimes\boldsymbol{S}^k=\frac{2\omega_g\Delta L}{3}\frac{\left|\boldsymbol{S}^k\right|^2\left(\left(\boldsymbol{u}_g'\right)^k\otimes\boldsymbol{u}_g^k\right)}{\left|\left(\boldsymbol{u}_g'\right)^k\right|^2}. \tag{55}$$

Based on (55), ΔL can be directly calculated as

$$\Delta L=\frac{1.5}{\omega_g}\frac{\left|\left(\boldsymbol{u}_g'\right)^k\right|^2\cdot\left(\left(\boldsymbol{u}_d^k\right)^*\boldsymbol{u}_g^k\right)\otimes\boldsymbol{S}^k}{\left|\boldsymbol{S}^k\right|^2\left(\left(\boldsymbol{u}_g'\right)^k\otimes\boldsymbol{u}_g^k\right)}. \tag{56}$$

However, direct calculation is sensitive to measurement noises. In order to obtain a smooth estimation, $\Delta\hat{L}$ can be calculated by integrating ΔL as

$$\begin{aligned}\Delta\hat{L}^{k+1}&=\Delta\hat{L}^k+hT_{sc}\Delta L\\&=\Delta\hat{L}^k+\frac{1.5hT_{sc}}{\omega_g}\frac{\left|\left(\boldsymbol{u}_g'\right)^k\right|^2\cdot\left(\left(\boldsymbol{u}_d^k\right)^*\boldsymbol{u}_g^k\right)\otimes\boldsymbol{S}^k}{\left|\boldsymbol{S}^k\right|^2\left(\left(\boldsymbol{u}_g'\right)^k\otimes\boldsymbol{u}_g^k\right)}\end{aligned} \tag{57}$$

where $h>0$ is a gain of the integrator. As analyzed in the previous section, $\hat{\boldsymbol{u}}_d^k$ can track $\boldsymbol{u}_d^k$ without error. Therefore, the estimated $\hat{\boldsymbol{u}}_d^k$ from the proposed DPDO is used to replace $\boldsymbol{u}_d^k$ in practical application. With estimation of the mismatched inductance, the estimated inductance $\hat{L}_g$ can be expressed as

$$\hat{L}_g=\hat{L}_0+\Delta\hat{L}^k \tag{58}$$

where $\hat{L}_0$ is the initialized grid-side inductance in the algorithm, which can be obtained by measurement with a meter or roughly set based on the developer's experience if it is unknown. With the proposed inductance estimation, the mismatch between $\hat{L}_0$ and the actual inductance L_g is online corrected, and thus, an accurate prior knowledge of the grid-side inductance is not required in the proposed method. According to (23) and (58), the mismatched inductance ΔL becomes

$$\Delta L^k=L_g-\hat{L}_0-\Delta\hat{L}^k. \tag{59}$$

Based on (56), (57), and (59), the relationship between $\Delta\hat{L}$ and $L_g-\hat{L}_0$ can be finally derived as

$$\frac{\Delta\hat{L}}{L_g-\hat{L}_0}=\frac{hT_{sc}}{z-1+hT_{sc}}. \tag{60}$$

It is seen that $\Delta\hat{L}$ is the low-pass-filtered value of the initial estimation error $L_g-\hat{L}_0$. The bandwidth of the low-pass filter is approximately h. Generally, inductance does not vary abruptly in practical applications. A smaller h is preferable for obtaining a smooth $\Delta\hat{L}$. In this paper, h is chosen as 50. Additionally, the incorporation of a low-pass filter can ensure the outer loop of inductance estimation works slower than the inner disturbance observer. This helps to decouple the interference between two loops. A complete block diagram of the proposed DPDO is shown in Fig. 2.

V. DPDO-Based Robust DPPC

The control diagram of the proposed DPDO-based DPPC is shown in Fig. 3. In this paper, only power control performance is concerned, and thus, the outer dc-link voltage control is not discussed in detail here.

Similarly, to make the complex power $\boldsymbol{S}$ reach the reference at the next sampling period, the converter voltage can be solved based on (29) as

$$\boldsymbol{u}_c^k=\boldsymbol{u}_g^k-\frac{2}{3}\left(\frac{(\hat{R}_g-\omega_g\hat{L}_gJ^k)\boldsymbol{S}^k}{\boldsymbol{u}_g^k}\right)^*-\frac{2\hat{L}_g}{3T_{sc}}\left(\frac{\boldsymbol{S}^{\mathrm{ref}}-\boldsymbol{S}^k}{\boldsymbol{u}_g^k}\right)^*-\boldsymbol{u}_d^k. \tag{61}$$

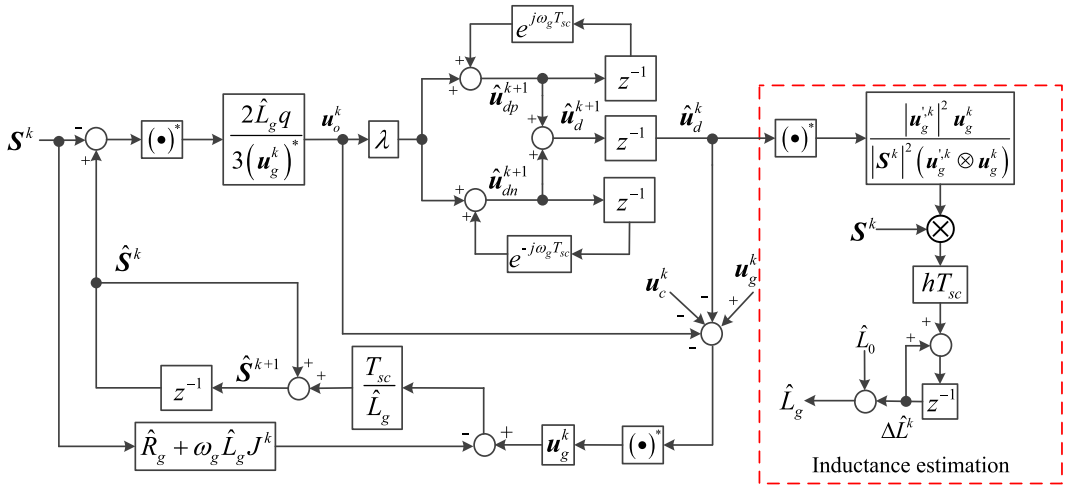

Fig. 2. Block diagram of the proposed DPDO.

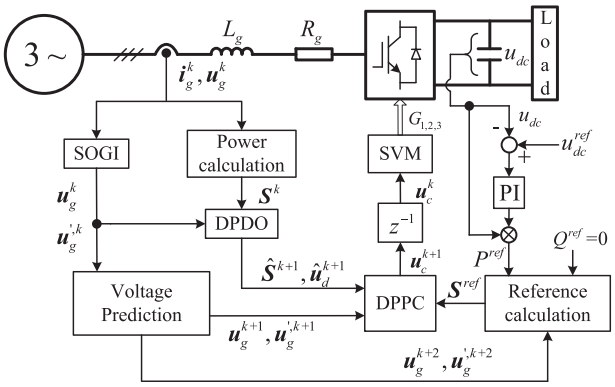

Fig. 3. Control diagram of DPDO-based DPPC.

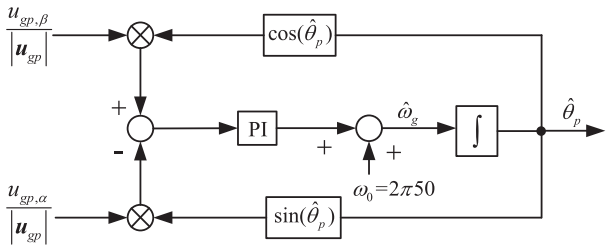

Fig. 4. Control diagram of the PLL for online frequency adaption.

According to (25), we have

$$\boldsymbol{u}_c^k = \hat{\boldsymbol{u}}_c^k - \boldsymbol{u}_d^k. \tag{62}$$

As $\boldsymbol{u}_d^k$ is unknown, its estimated value $\hat{\boldsymbol{u}}_d^k$ from the DPDO introduced in the previous section is used in (62) to calculate the control voltage. After getting $\boldsymbol{u}_c^k$, SVM is used to generate switching signals to control the rectifier. It is seen from (21) that the calculation of $\boldsymbol{S}^{\mathrm{ref}}$ requires a quadrature value of the grid voltage vector. In this paper, a second-order generalized integrator (SOGI) is used to get $\boldsymbol{u}_g^{'}$. More details about the SOGI can be found in [34], and thus, it is not repeated here. After obtaining $\boldsymbol{u}_g^{'}$, the FPSC of the grid voltage vector can be calculated as $\boldsymbol{u}_{gp} = 0.5(\boldsymbol{u}_g + j\boldsymbol{u}_g^{'})$. Based on the calculated $\boldsymbol{u}_{gp}$, a standard PLL can be employed for online grid frequency adaption, as shown in Fig. 4.

Typically, in the digital implementation, there is one-step delay between the calculated control voltage and the applied voltage. Similar to [2], [12], and [17], the control voltage at the $(k+1)$th instant is calculated for delay compensation. By shifting (61) one step ahead, the control voltage $\boldsymbol{u}_c^{k+1}$ can be obtained. It can be seen from (61) that the calculation of $\boldsymbol{u}_c^{k+1}$ requires $\boldsymbol{S}^{k+1}$, $\boldsymbol{u}_d^{k+1}$, $\boldsymbol{u}_g^{k+1}$, and power reference $\boldsymbol{S}^{\mathrm{ref}}$ at the $(k+2)$th instant. In the following text, the predictions of these variables will be introduced.

$\boldsymbol{u}_g^{k+1}$ can be simply predicted based on (15) as

$$\boldsymbol{u}_g^{k+1} = \boldsymbol{u}_g^k - \omega_g T_{sc}\left(\boldsymbol{u}_g^{'}\right)^k. \tag{63}$$

Similarly, $\left(\boldsymbol{u}_g^{'}\right)^{k+1}$ can be calculated as

$$\left(\boldsymbol{u}_g^{'}\right)^{k+1} = \left(\boldsymbol{u}_g^{'}\right)^k + \omega_g T_{sc}\boldsymbol{u}_g^k. \tag{64}$$

As can be seen from (33), $\hat{\boldsymbol{S}}^{k+1}$ and $\hat{\boldsymbol{u}}_d^{k+1}$ are directly available in the DPDO. As the designed DPDO can track the actual power accurately despite mismatched parameters, $\hat{\boldsymbol{S}}^{k+1}$ and $\hat{\boldsymbol{u}}_d^{k+1}$ are employed to replace $\boldsymbol{S}^{k+1}$ and $\boldsymbol{u}_d^{k+1}$ to compensate the one-step delay.

For better tracking performance, the complex power reference at $(k+2)$th instant should be predicted in practical application [11]. As seen from (21), $\boldsymbol{u}_g^{k+2}$ and $\left(\boldsymbol{u}_g^{'}\right)^{k+2}$ are required, which can be obtained by further shifting (63) and (64) one step ahead. Then, $\boldsymbol{S}^{\mathrm{ref}}$ can be calculated based on (21) as

$$\boldsymbol{S}^{\mathrm{ref}} = jP^{\mathrm{ref}}\frac{\left(\left(\boldsymbol{u}_g^{'}\right)^{k+2}\right)^*\boldsymbol{u}_g^{k+2}}{\boldsymbol{u}_g^{k+2}\otimes\left(\boldsymbol{u}_g^{'}\right)^{k+2}}. \tag{65}$$

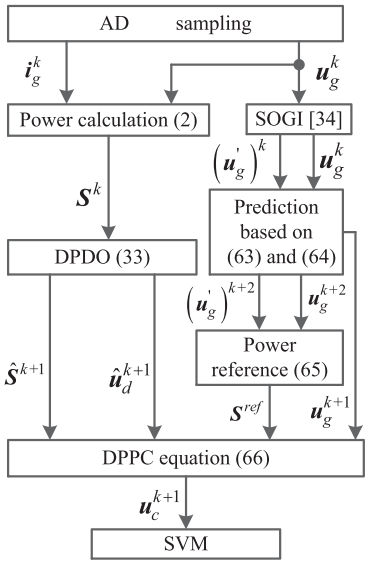

Fig. 5. Schematic diagram of the proposed control method.

Finally, the control voltage $\boldsymbol{u}_c^{k+1}$ with delay compensation can be expressed as

$$\boldsymbol{u}_c^{k+1} = \boldsymbol{u}_g^{k+1} - \frac{2}{3}\left(\frac{(\hat{R}_g - \omega_g \hat{L}_g J^{k+1})\hat{\boldsymbol{S}}^{k+1}}{\boldsymbol{u}_g^{k+1}}\right)^* - \frac{2\hat{L}_g}{3T_{sc}}\left(\frac{\boldsymbol{S}^{\mathrm{ref}} - \hat{\boldsymbol{S}}^{k+1}}{\boldsymbol{u}_g^{k+1}}\right)^* - \hat{\boldsymbol{u}}_d^{k+1}. \quad (66)$$

It should be noted that for a conventional DPPC under unbalanced grid conditions, the predictions of $\boldsymbol{S}^{k+1}$, $\boldsymbol{u}_g^{k+1}$, and $\boldsymbol{S}^{\mathrm{ref}}$ at the $(k+2)$th instant are also required to compensate for one-step delay. The difference is that in conventional methods, the complex power $\boldsymbol{S}^{k+1}$ is directly predicted based on the estimated system model (29). This will result in errors when there are model mismatches. However, in this paper, the complex power at the $(k+1)$th instant is obtained by a closed-loop DPDO, as shown in (33), which can provide accurate predictions even with model uncertainties. Since delay compensation and disturbance estimation are integrated together, the complexity is not substantially increased compared with the conventional DPPC, as also confirmed by the comparison of execution time shown in the next section. A schematic diagram of the proposed control algorithm is shown in Fig. 5.

VI. Experimental Results

Experimental tests on a two-level VSR were performed to verify the effectiveness of the proposed method. The system and control parameters are listed in Table I. The per-unit values are calculated with power base and voltage base selected as 1 kVA and 150 V, respectively. A 32-bit DSP TMS320F28335 is used to implement the whole algorithm. Experimental data are sampled by a scopecorder DL850. Chroma 61511, a programmable ac source, is used to provide unbalanced grid conditions. The whole experimental setup is shown in Fig. 6. A prior method presented in [18], which is named as prior DPPC in the following text,

TABLE I
System and Control Parameters

System parameters	Symbol	Value	p.u. value
Line resistance	R_g	0.3 Ω	0.0077
Line inductance	L_g	10 mH	0.0806
Line–line voltage	U_N	150 V	1
DC-link capacitor	C	840 μF	10.2842
Line voltage frequency	f_g	50 Hz	1
Load resistance	R_L	100 Ω	2.566
Sampling period	T_{sc}	100 μs	0.005
DPDO parameter 1	q	2000	N/A
DPDO parameter 2	λ	0.05	N/A

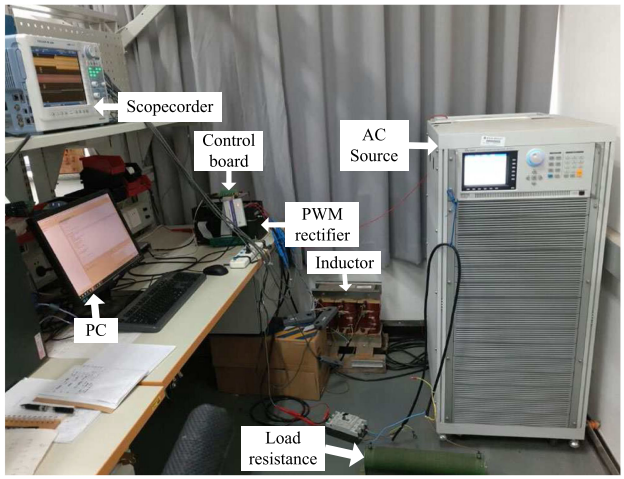

Fig. 6. Experimental test setup.

was also carried out for comparison. On the laboratory test rig, it takes 39.27 and 43.73 μs to execute algorithms of the prior DPPC and the proposed DPPC, respectively. Compared with the prior DPPC, the execution time is only increased by 4.46 μs, suggesting that the complexity is not substantially increased by incorporating the proposed disturbance observer and online inductance adaption. Considering the limitation of the execution time, the sampling frequency must be set below $1/43.73\,\mu s \approx 22.8$ kHz. In all the following experimental tests, the sampling frequency and the switching frequency are set as 10 kHz in order to obtain satisfactory performance with acceptable switching losses and sufficient time for executing the control algorithm. For the studied PWM rectifier, the minimum dc-link voltage should be larger than the peak value of line–line grid voltage. As shown in Table I, the peak line–line voltage for our test rig is $150\sqrt{2} \approx 212$ V. Considering that the load resistance is 100 Ω, the active power reference should be no smaller than $212^2/100 = 450$ W. Additionally, due to the limitation of the rated current, the active power reference is set below 1000 W. To avoid the influence of the outer dc voltage control loop on the inner power control, experimental tests were initially carried out by disconnecting the outer PI controller and the rectifier works in the power control mode. After verifying the superiority of the proposed DPPC, the voltage control mode is tested and the closed-loop dc voltage regulation is verified with a step change in the dc load.

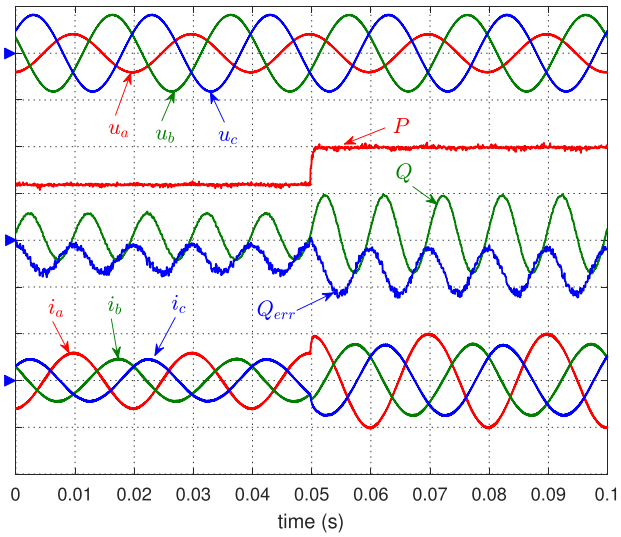

Fig. 7. Experimental results of prior DPPC when $\hat{L}_g = 0.5L_g$. u_{abc}: 150 V/div, P: 500 W/div, Q: 500 Var/div, $Q_{\rm err}$: 100 Var/div, and i_{abc} : 8 A/div.

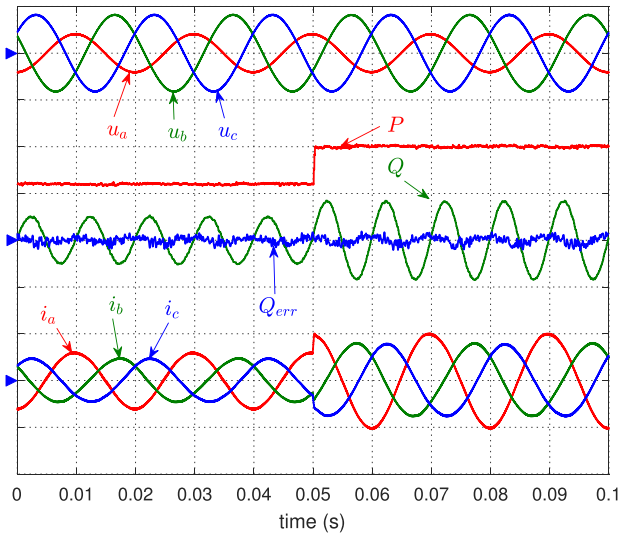

Fig. 9. Experimental results of DPDO-based DPPC with ΔL adaptation when $\hat{L}_0 = 0.5L_g$. u_{abc}: 150 V/div, P: 500 W/div, Q: 500 Var/div, $Q_{\rm err}$: 100 Var/div, and i_{abc} : 8 A/div.

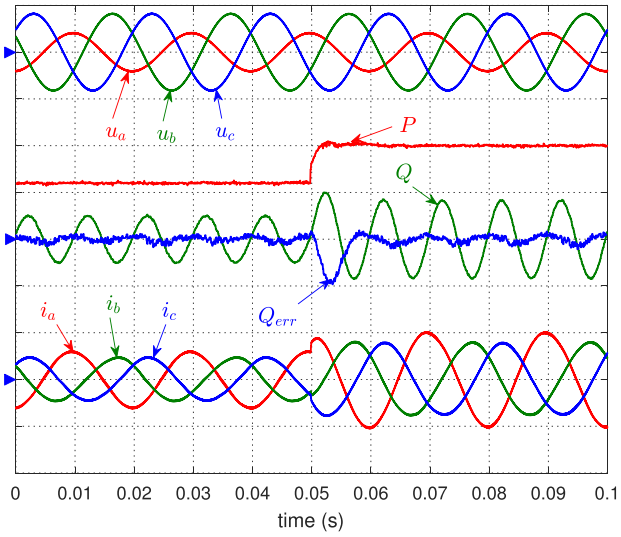

Fig. 8. Experimental results of DPDO-based DPPC without ΔL adaptation when $\hat{L}_0 = 0.5L_g$. u_{abc}: 150 V/div, P: 500 W/div, Q: 500 Var/div, $Q_{\rm err}$: 100 Var/div, and i_{abc} : 8 A/div.

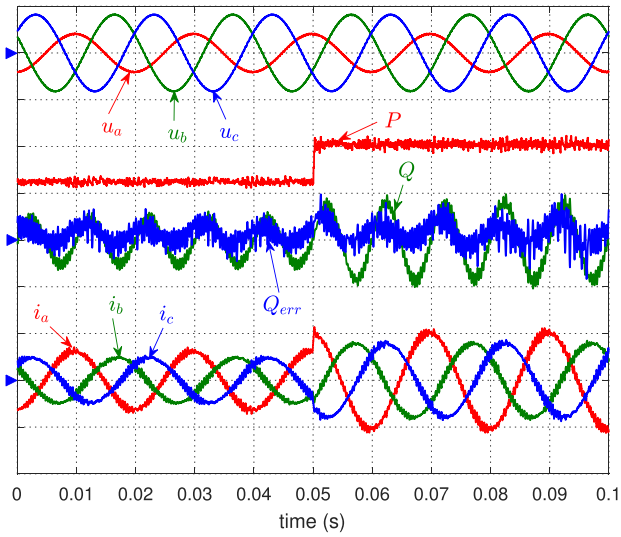

Fig. 10. Experimental results of prior DPPC when $\hat{L}_g = 2L_g$. u_{abc}: 150 V/div, P: 500 W/div, Q: 500 Var/div, $Q_{\rm err}$: 200 Var/div, and i_{abc} : 8 A/div.

Figs. 7–9 show the comparative results when the initial estimated inductance $\hat{L}_0$ is half of the actual value. Initially, $P^{\rm ref}$ is 600 W and then steps to 1000 W. And, 50% voltage dip in phase A is applied during the whole experimental tests. In the figure, $Q_{\rm err}$ is the tracking error of reactive power. It is seen that both methods can achieve constant active power and sinusoidal grid currents under unbalanced grid conditions. However, the prior DPPC is sensitive to the grid-side inductance mismatch, as analyzed in Section III-B. From Fig. 7, one can see that there is a significant deviation of reactive power for the prior DPPC, while from Fig. 8, it is seen that $Q_{\rm err}$ is around zero during the steady state for the DPDO-based DPPC. Though steady-state tracking accuracy is improved with DPDO, existence of ΔL will result in deteriorated dynamic performance as analyzed previously. It can be seen in Fig. 8 that there is a larger tracking error of the reactive power and slower tracking performance of the active power during transient process. Fig. 9 shows test results when ΔL is adapted online. The undesired transient responses shown in Fig. 8 do not exist when ΔL adaption is enabled. These tests confirm that the proposed DPDO can improve the tracking accuracy of DPPC under parameter mismatches. Further improvement can be made by online adaptation of inductance. Apparently, DPDO-based DPPC with online inductance estimation presents the best overall performance in this test.

Under the same conditions as previous tests, Figs. 10–12 illustrate comparative results when the initial estimated inductance $\hat{L}_0$ is twice of the actual value. For the prior DPPC as shown in Fig. 10, significant ripple components can be observed in the

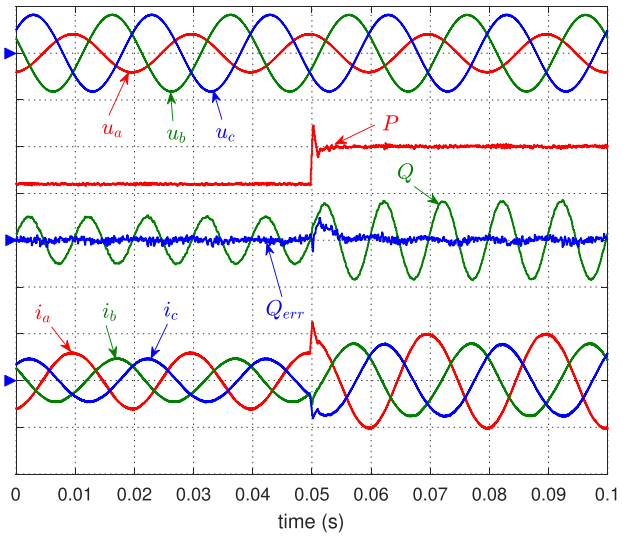

Fig. 11. Experimental results of DPDO-based DPPC without ΔL adaptation when $\hat{L}_0 = 2L_g$. u_{abc}: 150 V/div, P: 500 W/div, Q: 500 Var/div, $Q_{\rm err}$: 100 Var/div, and i_{abc} : 8 A/div.

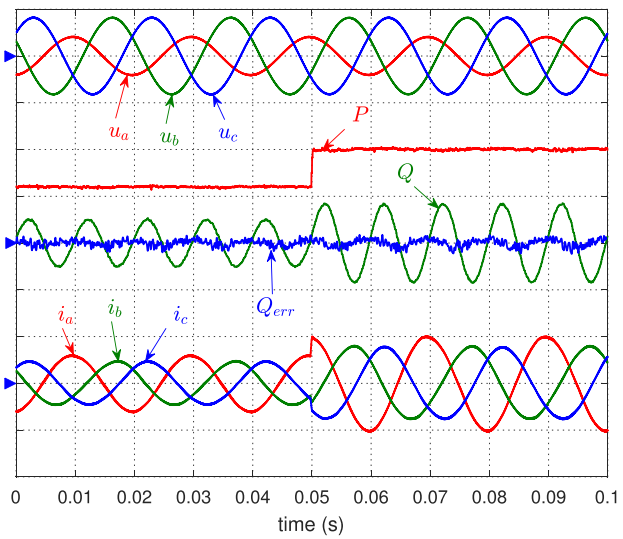

Fig. 12. Experimental results of DPDO-based DPPC with ΔL adaptation when $\hat{L}_0 = 2L_g$. u_{abc}: 150 V/div, P: 500 W/div, Q: 500 Var/div, $Q_{\rm err}$: 100 Var/div, and i_{abc} : 8 A/div.

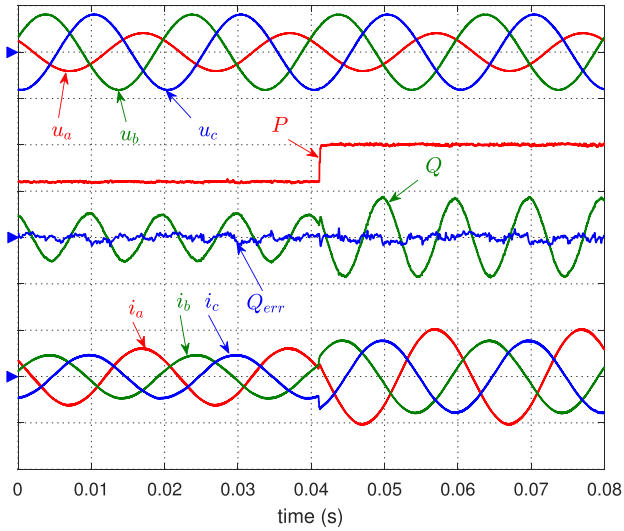

Fig. 13. Experimental results of DPDO-based DPPC with ΔL adaptation when $\hat{R}_g = 2R_g$ and $\hat{L}_0 = 0.5L_g$. u_{abc}: 150 V/div, P: 500 W/div, Q: 500 Var/div, $Q_{\rm err}$: 100 Var/div, and i_{abc} : 8 A/div.

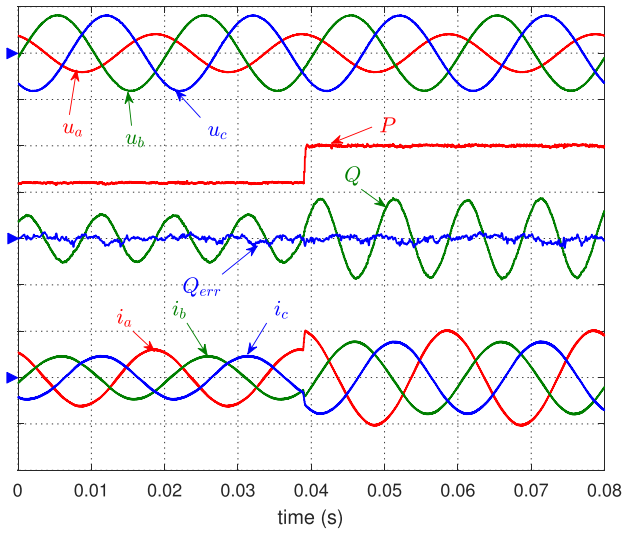

Fig. 14. Experimental results of DPDO-based DPPC with ΔL adaptation when $\hat{R}_g = 0.5R_g$ and $\hat{L}_0 = 2L_g$. u_{abc}: 150 V/div, P: 500 W/div, Q: 500 Var/div, $Q_{\rm err}$: 100 Var/div, and i_{abc} : 8 A/div.

recorded power and current waveforms, indicating that the control system is poorly damped in this test case. For DPDO-based DPPC without inductance estimation as shown in Fig. 11, the steady-state waveforms are smooth without harmonic components, and the average tracking error $Q_{\rm err}$ is zero. This test further confirms that DPDO can eliminate the steady-state tracking error in the DPPC when inductance mismatch exists. However, large overshoot can be seen in $P^{\rm ref}$ step responses. By contrast, when ΔL adaptation is enabled, DPDO-based DPPC shows superior performance over the prior DPPC and DPPC with only DPDO, as can be seen from the results shown in Fig. 12.

According to the above tests, it can be concluded that DPDO-based DPPC with ΔL adaptation has the best performance among three methods. In the following two tests, the influence of the resistance error ΔR will be evaluated. From analysis in [12], it can be seen that larger $\hat{R}_g$ with smaller $\hat{L}_0$ and smaller $\hat{R}_g$ with larger $\hat{L}_0$ can result in the worst working conditions. Hence, these two test cases were performed to verify the effectiveness of the proposed method. The results are shown in Figs. 13 and 14. It is seen that $Q_{\rm err}$ is nearly zero. Actual power P can track $P^{\rm ref}$ quickly with no significant overshoot during the transient process for both test cases.

Figs. 15–17 present responses of the proposed DPDO-based DPPC under two-phase voltage sag, three-phase voltage sag, and one-phase deep voltage sag conditions, respectively. In these tests, $P^{\rm ref} = 600$ W. With ideal grid voltages, it is seen that both

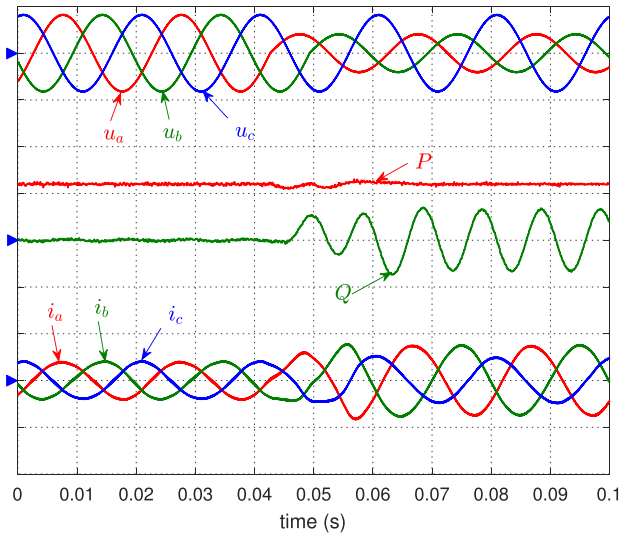

Fig. 15. Experimental results of DPDO-based DPPC with ΔL adaptation when 50% voltage dips in phase A and phase B are applied. u_{abc}: 150 V/div, P: 500 W/div, Q: 500 Var/div, and i_{abc} : 8 A/div.

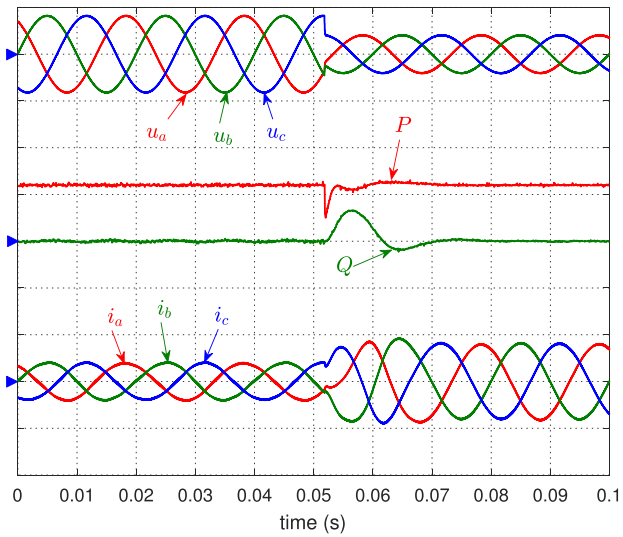

Fig. 16. Experimental results of DPDO-based DPPC with ΔL adaptation when 50% voltage dips in three phases are suddenly applied. u_{abc}: 150 V/div, P: 500 W/div, Q: 500 Var/div, and i_{abc} : 8 A/div.

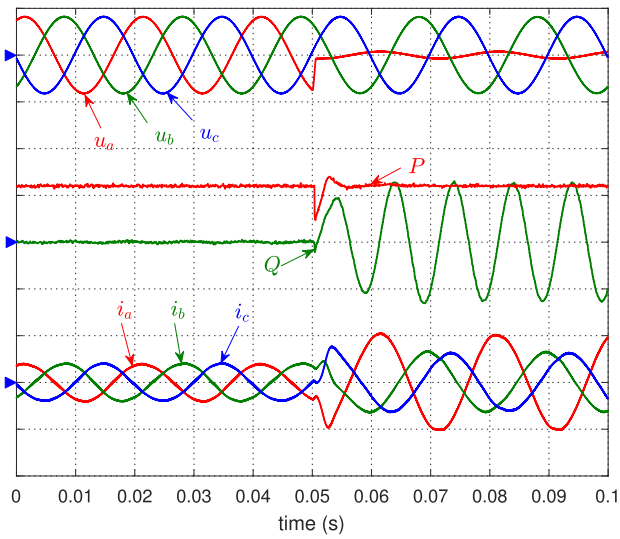

Fig. 17. Experimental results of DPDO-based DPPC with ΔL adaptation when 90% voltage dip in phase A is suddenly applied. u_{abc}: 150 V/div, P: 500 W/div, Q: 500 Var/div, and i_{abc} : 8 A/div.

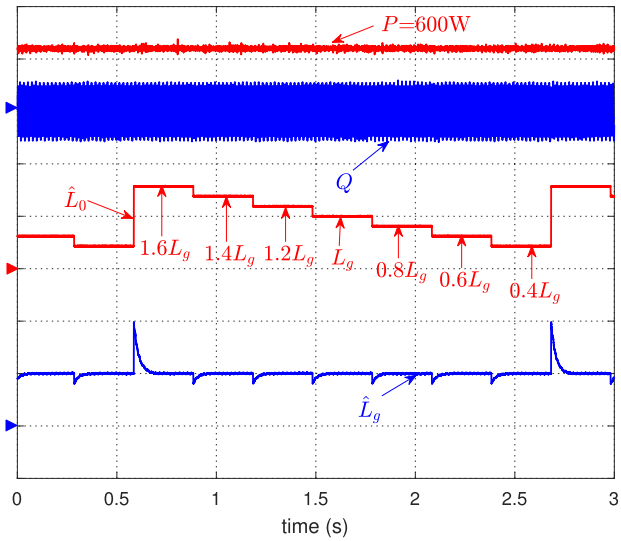

Fig. 18. Experimental results of DPDO based DPPC with ΔL adaptation when $\hat{L}_0$ varies from $1.6L_g$ to $0.4L_g$ under the unbalanced grid condition. P: 500 W/div, Q: 500 Var/div, $\hat{L}_0$: 10 mH/div, and $\hat{L}_g$: 10 mH/div.

active and reactive powers are kept constant at their references, and three-phase grid currents are balanced and sinusoidal. After voltage dip, active power P can return to its reference quickly, and twice of grid frequency oscillations can be observed in the reactive power when grid voltages are unbalanced. However, shapes of grid currents are still sinusoidal. Additionally, there is no inrush current when voltage sag suddenly occurs. The steady-state results are in accordance with that presented in [18] and [31]. These tests confirm that the proposed method can properly work under both ideal and severely unbalanced grid conditions.

The effectiveness of inductance estimation was also evaluated. Fig. 18 shows the estimated $\hat{L}_g$ when there is 50% voltage dip in phase A. During experimental tests, the real inductance is not changed but $\hat{L}_0$ is deliberately varied from $1.6L_g$ to $0.4L_g$. It can be found that $\hat{L}_g$ always converges to its actual value when $\hat{L}_0$ changes, indicating that the developed inductance adaptive scheme works well with different inductance errors.

Fig. 19 illustrates the experimental results when +5-Hz grid frequency change is suddenly applied under unbalanced grid conditions. When the grid frequency suddenly changes, there are some transient oscillations in both active and reactive powers. However, the system is stable and there is no inrush current. As the estimated grid frequency gradually converges to its actual value with the implemented PLL, the whole system can return to its normal operation after a sudden frequency change.

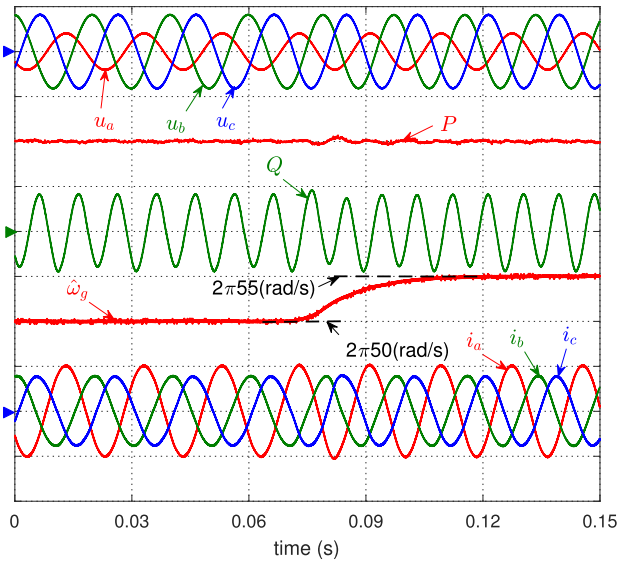

Fig. 19. Experimental results of the proposed DPPC with a step frequency change of +5 Hz under unbalanced grid conditions. u_{abc}: 150 V/div, P: 500 W/div, Q: 500 Var/div, $\hat{\omega}_g$: $2\pi5$ (rad/s)/div, and i_{abc} : 8 A/div.

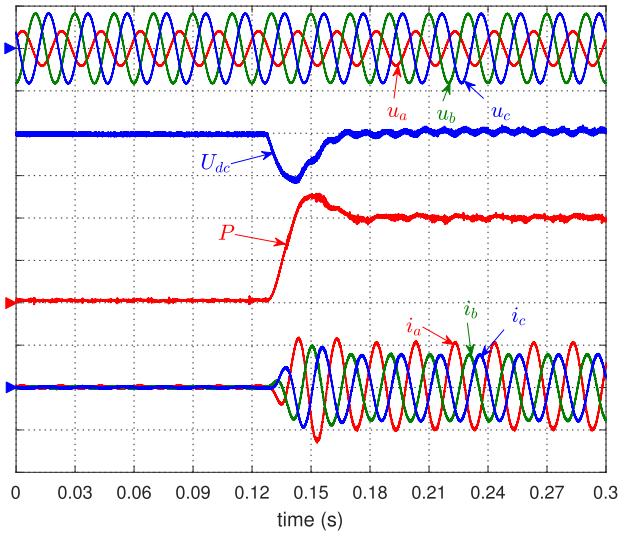

Fig. 20. Responses of the dc-link voltage when the external dc load is suddenly applied under unbalanced grid conditions. U_{dc}^{ref}: 300 V, u_{abc}: 150 V/div, P: 500 W/div, U_{dc}: 20 V/div, and i_{abc} : 8 A/div.

Finally, the effectiveness of the proposed DPPC is tested with closed-loop dc-link voltage regulation. In this test, the active power reference is generated by the outer PI controller, as shown in Fig. 3. The results when the external dc load is suddenly applied are depicted in Fig. 20. It can be found that when the external load is suddenly applied, the dc voltage can quickly return to its reference (300 V) after a drop. Although grid voltages are unbalanced, the active power is almost constant during the steady state and three-phase currents are sinusoidal. Due to the influence of the unbalanced grid voltages, there are minor oscillations at twice grid frequency in the dc-link voltage. To eliminate dc voltage oscillations, the control objective aiming at constant converter-side active power, as shown in [35], should be selected. However, there would be significant power ripples at input terminals. As this part is not the major concern of this paper, it will not be further expanded, and more details can be found in [35]. Harmonic spectrum of the obtained phase current during steady-state operation is shown in Fig. 21. The current total harmonic distortion (THD) is about 2.39%. Due to the use of SVM, high-order harmonics are mainly concentrated around multiplies of switching frequency (10 kHz).

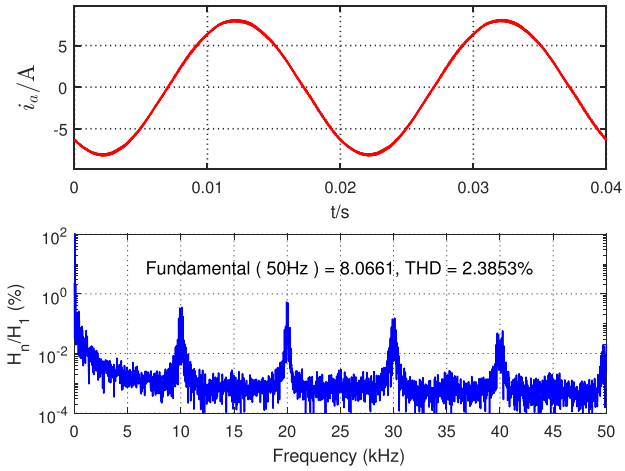

Fig. 21. Harmonic spectrum of phase current for the proposed DPPC.

VII. Conclusion

In this paper, a DPDO-based DPPC was proposed and experimentally verified with considerations of mismatched model parameters and unbalanced grid voltages. The designed DPDO can accurately estimate disturbance resulting from mismatched parameters. Stability and convergence as well as parameter tuning was theoretically analyzed. The DPDO was designed in the discrete-time domain, facilitating direct implementation in a digital controller. Due to the predictive ability of DPDO, delay compensation and disturbance estimation were simultaneously achieved. As a result, tracking accuracy can be improved with mismatched parameters without significantly complicating implementation when compared with a standard DPPC. To further improve dynamic performance, an inductance adaptation scheme was developed, which can accurately estimate the mismatched inductance with different initial errors. Experimental results and comparative studies validated that the DPDO-based DPPC with inductance estimation could achieve satisfactory steady-state and dynamic performance under different parameter mismatches.

Appendix

During steady-state operation, $\boldsymbol{S}^k = \boldsymbol{S}^{\text{ref}}$. According to (20), the following equation can be derived:

$$\boldsymbol{S}^{k+1} - \boldsymbol{S}^k = jP\left(\frac{\boldsymbol{u}_g^{k+1}\odot\boldsymbol{u}_g^{q,k+1}}{\boldsymbol{u}_g^{k+1}\otimes\boldsymbol{u}_g^{q,k+1}} - \frac{\boldsymbol{u}_g^{k}\odot\boldsymbol{u}_g^{q,k}}{\boldsymbol{u}_g^{k}\otimes\boldsymbol{u}_g^{q,k}}\right). \quad (67)$$

For two complex vectors A and B, $A\otimes jB = A\odot B$. Hence, $\boldsymbol{u}_g\otimes\boldsymbol{u}_g^q$ and $\boldsymbol{u}_g\odot\boldsymbol{u}_g^q$ can be expanded in terms of $\boldsymbol{u}_{gp}$ and

$\boldsymbol{u}_{gn}$ as

$$\boldsymbol{u}_g \otimes \boldsymbol{u}_g^q = (\boldsymbol{u}_{gp} + \boldsymbol{u}_{gn}) \otimes (-j\boldsymbol{u}_{gp} + j\boldsymbol{u}_{gn}) \tag{68}$$

$$= |\boldsymbol{u}_{gn}|^2 - |\boldsymbol{u}_{gp}|^2 \tag{69}$$

$$\boldsymbol{u}_g \odot \boldsymbol{u}_g^q = (\boldsymbol{u}_{gp} + \boldsymbol{u}_{gn}) \odot (-j\boldsymbol{u}_{gp} + j\boldsymbol{u}_{gn}) \tag{70}$$

$$= 2\boldsymbol{u}_{gn} \otimes \boldsymbol{u}_{gp}. \tag{71}$$

It can be seen that $\boldsymbol{u}_g \otimes \boldsymbol{u}_g^q$ is a constant during steady-state operation. In the following text, variable M is used to replace $\boldsymbol{u}_g \otimes \boldsymbol{u}_g^q$ for simplicity, i.e.,

$$M = \boldsymbol{u}_g \otimes \boldsymbol{u}_g^q = |\boldsymbol{u}_{gn}|^2 - |\boldsymbol{u}_{gp}|^2 . \tag{72}$$

Equation (67) can then be rewritten as

$$\boldsymbol{S}^{k+1} - \boldsymbol{S}^k = \frac{2jP\left[\left(\boldsymbol{u}_{gn}^{k+1} \otimes \boldsymbol{u}_{gp}^{k+1}\right) - \left(\boldsymbol{u}_{gn}^{k} \otimes \boldsymbol{u}_{gp}^{k}\right)\right]}{M}. \tag{73}$$

With a small sampling period, $\boldsymbol{u}_{gn}^{k+1} = \boldsymbol{u}_{gn}^k \left(1 - j\omega_g T_{sc}\right)$ and $\boldsymbol{u}_{gp}^{k+1} = \boldsymbol{u}_{gp}^k \left(1 + j\omega_g T_{sc}\right)$. Neglecting T_{sc}^2 related terms, (73) can be simplified as

$$\boldsymbol{S}^{k+1} - \boldsymbol{S}^k = jPT_{sc}\frac{4\omega_g \boldsymbol{u}_{gp}^k \odot \boldsymbol{u}_{gn}^k}{M}. \tag{74}$$

According to (21) and (69), we have

$$J^k \omega_g \boldsymbol{S}^k = jP^{\mathrm{ref}}\frac{\omega_g \left|\boldsymbol{u}_g^{q,k}\right|^2}{M}$$

$$= j\omega_g P\frac{\left|\boldsymbol{u}_{gn}^k\right|^2 + \left|\boldsymbol{u}_{gp}^k\right|^2 - 2\boldsymbol{u}_{gp}^k \odot \boldsymbol{u}_{gn}^k}{M}. \tag{75}$$

Based on (74) and (75), (31) can be rewritten as

$$\boldsymbol{u}_d^k = \frac{2\omega_g \Delta L}{3}\left(\frac{jP\left|\boldsymbol{u}_g^k\right|^2}{M\boldsymbol{u}_g^k}\right)^* + \frac{2}{3}\Delta R\left(\frac{\boldsymbol{S}^k}{\boldsymbol{u}_g^k}\right)^*. \tag{76}$$

From (21), we obtain

$$\left(\frac{\boldsymbol{S}^k}{\boldsymbol{u}_g^k}\right)^* = -jP\left(\frac{j\boldsymbol{u}_{gn} - j\boldsymbol{u}_{gp}}{M}\right).$$

Considering $\left|\boldsymbol{u}_g^k\right|^2 = \left(\boldsymbol{u}_g^k\right)^* \boldsymbol{u}_g^k$, (76) can then be rearranged as

$$\boldsymbol{u}_d^k = \frac{2}{3}P\frac{j\omega_g \Delta L\left(\boldsymbol{u}_{gp} + \boldsymbol{u}_{gn}\right) + \Delta R\left(\boldsymbol{u}_{gp} - \boldsymbol{u}_{gn}\right)}{M}$$

$$= \frac{2P\left[\left(j\omega_g \Delta L + \Delta R\right)\boldsymbol{u}_{gp} + \left(j\omega_g \Delta L - \Delta R\right)\boldsymbol{u}_{gn}\right]}{3M}. \tag{77}$$

It is clear that $\boldsymbol{u}_d^k$ consists of the following FPSC $\boldsymbol{u}_{dp}^k$ and FNSC $\boldsymbol{u}_{dn}^k$:

$$\boldsymbol{u}_{dp}^k = \frac{2P\left(j\omega_g \Delta L + \Delta R\right)}{3M}\boldsymbol{u}_{gp}, \tag{78}$$

$$\boldsymbol{u}_{dn}^k = \frac{2P\left(j\omega_g \Delta L - \Delta R\right)}{3M}\boldsymbol{u}_{gn}. \tag{79}$$

REFERENCES

[1] S. Vazquez *et al.*, "Model predictive control: A review of its applications in power electronics," *IEEE Ind. Electron. Mag.*, vol. 8, no. 1, pp. 16–31, Mar. 2014.

[2] Y. Zhang, J. Gao, and C. Qu, "Relationship between two direct power control methods for PWM rectifiers under unbalanced network," *IEEE Trans. Power Electron.*, vol. 32, no. 5, pp. 4084–4094, May 2017.

[3] V. Blasko and V. Kaura, "A new mathematical model and control of a three-phase AC-DC voltage source converter," *IEEE Trans. Power Electron.*, vol. 12, no. 1, pp. 116–123, Jan. 1997.

[4] Z. Yingchao, Z. Zhengming, Z. Yongchang, L. Ting, and Y. Liqiang, "The virtual flux oriented control of three-level neutral point clamped PWM rectifier," in *Proc. Int. Conf. Electr. Mach. Syst.*, Oct. 2007, pp. 22–27.

[5] Y. Zhang and C. Qu, "Table-based direct power control for three-phase AC/DC converters under unbalanced grid voltages," *IEEE Trans. Power Electron.*, vol. 30, no. 12, pp. 7090–7099, Dec. 2015.

[6] A. M. Razali, M. A. Rahman, G. George, and N. A. Rahim, "Analysis and design of new switching lookup table for virtual flux direct power control of grid-connected three-phase PWM AC-DC converter," *IEEE Trans. Ind. Appl.*, vol. 51, no. 2, pp. 1189–1200, Mar. 2015.

[7] Y. Zhang and C. Qu, "Model predictive direct power control of PWM rectifiers under unbalanced network conditions," *IEEE Trans. Ind. Electron.*, vol. 62, no. 7, pp. 4011–4022, Jul. 2015.

[8] J. Rodriguez *et al.*, "State of the art of finite control set model predictive control in power electronics," *IEEE Trans. Ind. Informat.*, vol. 9, no. 2, pp. 1003–1016, May 2013.

[9] A. G. Yepes, A. Vidal, J. Malvar, O. Lòpez, and J. Doval-Gandoy, "Tuning method aimed at optimized settling time and overshoot for synchronous proportional-integral current control in electric machines," *IEEE Trans. Power Electron.*, vol. 29, no. 6, pp. 3041–3054, Jun. 2014.

[10] A. Bouafia, J. P. Gaubert, and F. Krim, "Predictive direct power control of three-phase pulsewidth modulation (PWM) rectifier using space-vector modulation (SVM)," *IEEE Trans. Power Electron.*, vol. 25, no. 1, pp. 228–236, Jan. 2010.

[11] J. Rodriguez and P. Cortes, *Predictive Control of Power Converters and Electrical Drives*, vol. 37. New York, NY, USA: Wiley–IEEE Press, 2012.

[12] H. A. Young, M. A. Perez, and J. Rodriguez, "Analysis of finite-control-set model predictive current control with model parameter mismatch in a three-phase inverter," *IEEE Trans. Ind. Electron.*, vol. 63, no. 5, pp. 3100–3107, May 2016.

[13] C. Xia, M. Wang, Z. Song, and T. Liu, "Robust model predictive current control of three-phase voltage source PWM rectifier with online disturbance observation," *IEEE Trans. Ind. Informat.*, vol. 8, no. 3, pp. 459–471, Aug. 2012.

[14] Z. Song, Y. Tian, W. Chen, Z. Zou, and Z. Chen, "Predictive duty cycle control of three-phase active-front-end rectifiers," *IEEE Trans. Power Electron.*, vol. 31, no. 1, pp. 698–710, Jan. 2016.

[15] J. S. Lee and R. D. Lorenz, "Robustness analysis of deadbeat-direct torque and flux control for IPMSM drives," *IEEE Trans. Ind. Electron.*, vol. 63, no. 5, pp. 2775–2784, May 2016.

[16] Y. Zhang, Y. Bai, and H. Yang, "A universal multiple-vector-based model predictive control of induction motor drives," *IEEE Trans. Power Electron.*, 2017, to be published.

[17] W. Song, J. Ma, L. Zhou, and X. Feng, "Deadbeat predictive power control of single-phase three-level neutral-point-clamped converters using space-vector modulation for electric railway traction," *IEEE Trans. Power Electron.*, vol. 31, no. 1, pp. 721–732, Jan. 2016.

[18] Y. Zhang and C. Qu, "Direct power control of a pulse width modulation rectifier using space vector modulation under unbalanced grid voltages," *IEEE Trans. Power Electron.*, vol. 30, no. 10, pp. 5892–5901, Oct. 2015.

[19] S. Kwak, U. C. Moon, and J. C. Park, "Predictive-control-based direct power control with an adaptive parameter identification technique for improved AFE performance," *IEEE Trans. Power Electron.*, vol. 29, no. 11, pp. 6178–6187, Nov. 2014.

[20] B. Arif, L. Tarisciotti, P. Zanchetta, J. C. Clare, and M. Degano, "Grid parameter estimation using model predictive direct power control," *IEEE Trans. Ind. Appl.*, vol. 51, no. 6, pp. 4614–4622, Nov. 2015.

[21] W. Song, Z. Deng, S. Wang, and X. Feng, "A simple model predictive power control strategy for single-phase PWM converters with modulation function optimization," *IEEE Trans. Power Electron.*, vol. 31, no. 7, pp. 5279–5289, Jul. 2016.

[22] D. Martin and E. Santi, "Autotuning of digital deadbeat current controllers for grid-tie inverters using wide bandwidth impedance identification," *IEEE Trans. Ind. Appl.*, vol. 50, no. 1, pp. 441–451, Jan. 2014.

[23] S. K. Kim, D. K. Choi, K. B. Lee, and Y. I. Lee, "Offset-free model predictive control for the power control of three-phase AC/DC converters," *IEEE Trans. Ind. Electron.*, vol. 62, no. 11, pp. 7114–7126, Nov. 2015.

[24] S. K. Kim, "Offset-free one-step ahead state predictor for power electronic applications using robust proportional-integral observer," *IEEE Trans. Ind. Electron.*, vol. 63, no. 3, pp. 1763–1770, Mar. 2016.

[25] K. J. Lee, B. G. Park, R. Y. Kim, and D. S. Hyun, "Robust predictive current controller based on a disturbance estimator in a three-phase grid-connected inverter," *IEEE Trans. Power Electron.*, vol. 27, no. 1, pp. 276–283, Jan. 2012.
[26] X. Zhang, B. Hou, and Y. Mei, "Deadbeat predictive current control of permanent-magnet synchronous motors with stator current and disturbance observer," *IEEE Trans. Power Electron.*, vol. 32, no. 5, pp. 3818–3834, May 2017.
[27] Z. Dai and W. Lin, "Adaptive estimation of three-phase grid voltage parameters under unbalanced faults and harmonic disturbances," *IEEE Trans. Power Electron.*, vol. 32, no. 7, pp. 5613–5627, Jul. 2017.
[28] J. R. Fischer, S. A. González, I. Carugati, M. A. Herrán, M. G. Judewicz, and D. O. Carrica, "Robust predictive control of grid-tied converters based on direct power control," *IEEE Trans. Power Electron.*, vol. 29, no. 10, pp. 5634–5643, Oct. 2014.
[29] H. Yang, Y. Zhang, J. Liang, J. Gao, P. D. Walker, and N. Zhang, "Sliding-mode observer based voltage-sensorless model predictive power control of PWM rectifier under unbalanced grid conditions," *IEEE Trans. Ind. Electron.*, vol. 65, no. 7, pp. 5550–5560, Jul. 2018.
[30] Y. Suh and T. A. Lipo, "Control scheme in hybrid synchronous stationary frame for PWM AC/DC converter under generalized unbalanced operating conditions," *IEEE Trans. Ind. Appl.*, vol. 42, no. 3, pp. 825–835, May 2006.
[31] K. Ma, W. Chen, M. Liserre, and F. Blaabjerg, "Power controllability of a three-phase converter with an unbalanced AC source," *IEEE Trans. Power Electron.*, vol. 30, no. 3, pp. 1591–1604, Mar. 2015.
[32] H. Yang, Y. Zhang, J. Liang, N. Zhang, and P. Walker, "A robust deadbeat predictive power control with sliding mode disturbance observer for PWM rectifiers," in *Proc. IEEE Energy Convers. Congr. Expo.*, Cincinnati, OH, USA, Oct. 2017, pp. 4595–4600.
[33] K. Ogata, *Discrete-Time Control Systems*, vol. 2. Englewood Cliffs, NJ, USA: Prentice-Hall, 1995.
[34] P. Rodríguez, A. Luna, R. S. M. noz Aguilar, I. Etxeberria-Otadui, R. Teodorescu, and F. Blaabjerg, "A stationary reference frame grid synchronization system for three-phase grid-connected power converters under adverse grid conditions," *IEEE Trans. Power Electron.*, vol. 27, no. 1, pp. 99–112, Jan. 2012.
[35] Y. Zhang, J. Liu, H. Yang, and J. Gao, "Direct power control of pulse width modulated rectifiers without DC voltage oscillations under unbalanced grid conditions," *IEEE Trans. Ind. Electron.*, 2018, to be published.

Haitao Yang (S' 16) received the B.S. degree from the Hefei University of Technology, Hefei, China, in 2009, and the M.S. degree from the North China University of Technology, Beijing, China, in 2015, both in electrical engineering. He is currently working toward the Ph.D. degree in mechanical engineering at the School of Mechanical and Mechatronic Engineering, University of Technology Sydney, Ultimo, NSW, Australia.

His research interests include motor drives, position/speed sensorless control of ac motors, pulsewidth modulation converters, and electric vehicles.

Yongchang Zhang (M'10–SM'18) received the B.S. degree from Chongqing University, Chongqing, China, in 2004, and the Ph.D. degree from Tsinghua University, Beijing, China, in 2009, both in electrical engineering.

From August 2009 to August 2011, he was a Postdoctoral Fellow with the University of Technology Sydney, Ultimo, NSW, Australia. In August 2011, he joined the North China University of Technology, Beijing, as an Associate Professor. He is currently a Full Professor and the Director of the Inverter Technologies Engineering Research Center of Beijing, Beijing. He has authored or coauthored more than 100 technical papers in the area of motor drives, pulsewidth modulation, and ac/dc converters. His current research interests include model-predictive control for power converters and motor drives.

Jiejunyi Liang received the B.S. degree in mechanical design, manufacturing, and automation from the Huazhong University of Science and Technology, Wuhan, China, in 2012, and the M.S. degree in electromechanical engineering from the University of Macau, Macau, China, in 2015. He is currently working toward the Ph.D. degree in mechanical engineering at the School of Mechanical and Mechatronic Engineering, University of Technology Sydney, Ultimo, NSW, Australia.

Jie Liu was born in 1992. He received the B.S. degree in automation engineering from the North China University of Technology, Beijing, China, in 2015, where he is currently working toward the M.S. degree in control science and engineering.

His research interests include control of pulsewidth modulation rectifiers.

Nong Zhang received the Ph.D. degree from the University of Tokyo, Tokyo, Japan, in 1989.

He worked with several universities in China, Japan, the United States, and Australia before joining the University of Technology Sydney, Ultimo, NSW, Australia, in 1995, where he has been a Professor of mechanical engineering at the School of Mechanical and Mechatronic Engineering, since 2009. He developed advanced models and numerical schemes for simulating gear shift in powertrains with automatic transmission, manual transmission, and continuously variable transmission and for dynamic analysis of vehicles fitted with advanced suspensions. His research interests include mechanical vibration, multibody system dynamics, and its applications to complex machines and vehicular systems.

Paul D. Walker was born in Sydney, NSW, Australia, in 1981. He received the B.E. and Ph.D. degrees in mechanical engineering from the University of Technology Sydney (UTS), Ultimo, NSW, in 2007 and 2011, respectively.

Since 2011, he has been a Research Associate and is currently a Senior Lecturer at the School of Mechanical and Mechatronic Engineering, UTS. His research interests include the development of novel power-splitting transmissions for hybrid electric vehicles, multispeed transmission dynamics and control, and novel hybrid and electric vehicle topologies and their control.